Surface & Coatings Technology 204 (2009) 988–991

Contents lists available at ScienceDirect

Surface & Coatings Technology

journal homepage: www.elsevier.com/locate/surfcoat

BGA cutter improvement utilizing nano-TiAlN coating layers synthesized by cathodic arc ion plating process

Sung-Hsiu Huang [a], Tsung-Eong Hsieh [a,*], Jia-Wei Chen [b]

[a] Department of Materials Science and Engineering, National Chiao Tung University, 1001, Ta-Hsueh Road, Hsinchu, 300, Taiwan, ROC
[b] Gigastorage Corporation, 3, Kung-Yeh First Road, Hsinchu Industrial Park, Hsinchu, 310, Taiwan, ROC

ARTICLE INFO

Available online 15 May 2009

Keywords:
TiAlN
Nanocomposite
Cathodic arc ion plating
BGA cutter
TEM

ABSTRACT

Ti/Al targets with various concentration ratios, $Ti_{0.75}Al_{0.25}$, $Ti_{0.66}Al_{0.33}$, $Ti_{0.5}Al_{0.5}$ and $Ti_{0.33}Al_{0.66}$ were used in a filtered cathodic arc ion plating system (FCAIP) to deposit the multilayer TiAlN films on Si wafer substrates and WC cermet ball grid array (BGA) cutters at various modulation wavelengths. Transmission electron microscopy (TEM), nanoindentation and BGA router were used to evaluate the characteristics of TiAlN layers and the performance of BGA cutters. TEM analysis revealed that the modulation wavelengths of deposited layers are less than 10 nm at various rotation speeds in FCAIP chamber and the crystal structure of TiAlN layer with the maximum hardness is NaCl-B1 structure using the $Ti_{0.5}Al_{0.5}$ target. The maximum hardness of multiple TiAlN layers measured by nanoindentation was 43 GPa, while the TiAlN monolayer exhibited the maximum hardness of 30 GPa in the same chamber. The TiAlN-coated BGA cutter deposited at the optimized condition exhibited a twice longer life and a higher machining speed in comparison with the conventional cutter.

1. Introduction

The depaneling and slotting process of printed circuit board (PCB), ball grid array (BGA) and flip chip (FC) substrates is an innovative cutting application requiring a high cutting speed, dry machining and high accuracy. Based on such heavy machining requirements, tungsten carbide (WC) cermet tools are widely used. In the meantime, titanium aluminum nitride (TiAlN) coating on the WC tools by filtered cathodic arc ion plating system (FCAIP) has the superior properties of hardness, wear resistance and higher oxidation temperature which offer proven benefits in terms of tool life and machining performance [1–3].

Recently, different approaches to the preparation of superhard coatings by physical vapor deposition (PVD) provide the coating films with a higher hardness, such as energetic ion bombardment during deposition [4,5], nanostructured superhard by spinodal phase segregation [6–8], *etc*. Moreover, the multilayer coatings consisting of different transition metal nitrides have received a lot of interest due to their higher hardness at a low bilayer thickness [9–11]. The most important features of multilayer superhard coatings are the presence of a lattice mismatch between the adjacent materials. Therefore most of the multilayer coatings were investigated on different transition metal nitrides such as TiN/ZrN, TiN/CrN and TiAlN/NbN [12]. Several reports proposed that the mechanical properties of their coatings are enhanced by the lattice mismatch between the constituent materials providing the coherency-strains to constrain the dislocation activity [13]. The residual stress between the nanolayers would also increase the possibility of peering during machining. In order to improve the adhesive properties, in the present study the Ti/Al targets with various concentration ratios were used in FCAIP to deposit the multilayer TiAlN films on Si wafer substrate and WC cermet BGA cutters at various modulation wavelengths by adjusting the rotation speeds. Their nanoindentation hardness, machining performance, thermal stability and microstructure were also studied.

2. Experimental

The multilayer TiAlN coatings were deposited onto WC cermet tools (BGA micro cutter with 1.0 mm in diameter made by Union Corporation, Japan) and silicon (100) substrates by FCAIP comprised of three cathodes with linear filters as shown in Fig. 1. The TiAl alloy targets with various compositions, as shown in Table 1, were mounted on each side of the cathode, while the nano-scale multilayer structure was deposited by the rotation of the holder and the revolution of the main spindle. The tools and substrates were chemically cleaned in an ultrasonic agitator containing surfactant and DI water. Subsequently, the specimens were cleaned *in-situ* by Ar^+ ion bombardment for 15 min, while a DC bias of −750 V was applied to the substrate at Ar pressure of 1×10^{-2} Torr. Before the reactive gas of N_2 was fed into the chamber, the specimens were cleaned by metal ion etching with high DC bias. After that, the reactive gas of N_2 was fed and the DC bias was decreased to -100 V step by step to enhance the adhesion of coating layers on the specimens. The multilayer TiAlN films were prepared from the reactive ion deposition of various concentrations of TiAl, as

* Corresponding author. Tel.: +886 3 5712121x55306; fax: +886 3 5724727.
E-mail address: tehsieh@mail.nctu.edu.tw (T.-E. Hsieh).

0257-8972/$ – see front matter © 2009 Elsevier B.V. All rights reserved.
doi:10.1016/j.surfcoat.2009.05.014

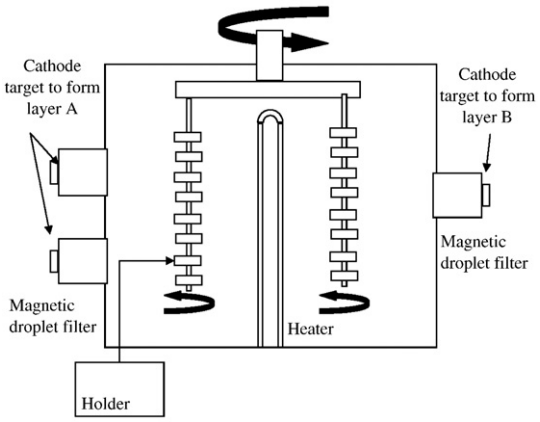

Fig. 1. Schematic diagram of the FCAIP system.

shown in Table 1, in $Ar+N_2$ plasma operated at a pressure of 6×10^{-3} Torr.

The nanoindentation hardness was measured by Hystron TriboScope using a Berkovich diamond indenter with 2000 nN load. Indentation load was constrained for decreasing the influence of the substrate; the ratio of the indentation depth to the film thickness was kept smaller than 10% [5]. In this study, the indentation depths of various coatings were around 30 nm. Area function was calibrated by fuse quartz and was applied in the hardness calculation according to the Oliver–Pharr method [15]. After the nanoindentation hardness of various coatings were measured, the coated substrate and BGA cutter with the highest hardness were investgated by machining performance and microstructure analysis in the sequence stage.

The machining performance of the TiAlN nanolayer-coated cutting tools was assessed on PCB routing machine (model: PR2228-S4 made by Anderson Machining Group, Taiwan). The cutting workpiece was bismaleimide triazine (BT) resin substrate (model: HL832NX (EX) with copper foil made by Mitsubishi Gas Chemical, Inc.) which is the major resin substrate used in BGA modulus and FC substrate. The cutters (diameter = 1.0 mm) designed for BGA depaneling and slotting process were made by Taiwan Union Tool Co. The computerized program of the cutting route simulated the BGA slotting process with spindle rotation of 45,000 rpm, feeding table speed of 20 mm/min and 30 cm length for each slot. The performance of the cutter was determined by the machining distance and the slot accuracy before it was broken.

In order to test the thermal stability of the TiAlN multilayer films, the multilayer- and monolayer-coated Si substrates were simultaneously heated in air in a furnace at T_A = 200–900 °C. The annealing treatment cycle was held at a rapid heating rate of 10 °C/min, followed by soaking at the desired temperature for 30 min and then cooled down at a rate of 10 °C/min. The mechanical properties changed as a result of heating were measured using the nanoindentation tester.

Table 1
Mechanical properties of various coatings deposited with various target compositions.

Condition no.	Target A (Ti:Al at.%)	Target B (Ti:Al at.%)	Arc current (amp)	Deposition time (min)	Rotation speed (rpm)	Hardness (GPa)[a]	Young's modulus (GPa)
S1	50%:50%	50%:50%	70	18	2	27.4	245.9
S2	75%:25%	75%:25%	70	18	2	25.01	236.6
S3	33%:66%	33%:66%	70	18	2	22.48	200.9
S4	33%:66%	66%:33%	70	18	2	24.05	213.2
S5	33%:66%	75%:25%	70	18	2	22.1	251.1
S6	50%:50%	33%:66%	70	18	2	41.4	251.8
S7	50%:50%	33%:66%	70	18	4	43.9	255.8

[a] Nanoindent load: 2000 nN.

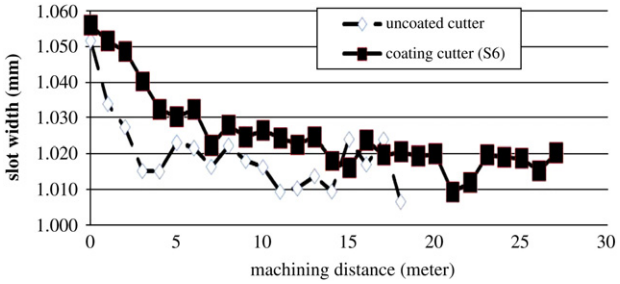

Fig. 2. Slot width versus the machining distance of coated and uncoated BGA cutters.

Cross-sectional TEM (XTEM) specimens were prepared by focused ion beam (FIB) method using the Si substrate coated with the highest hardness film. The samples were examined in a Philips Tecnai S-TWIN field emission gun TEM operated at 200 kV and the selected area electron diffraction (SAED) was used to identify the crystal structure of the coatings.

3. Results and discussion

Table 1 shows the nanoindentation hardness of various coatings deposited with various target alloy concentrations where Ti/Al ratios were varied with 75/25, 66/33, 50/50 and 33/66. The nanoindentation hardness of monolayer TiAlN film deposited by $Ti_{0.5}Al_{0.5}$ alloy (S1)

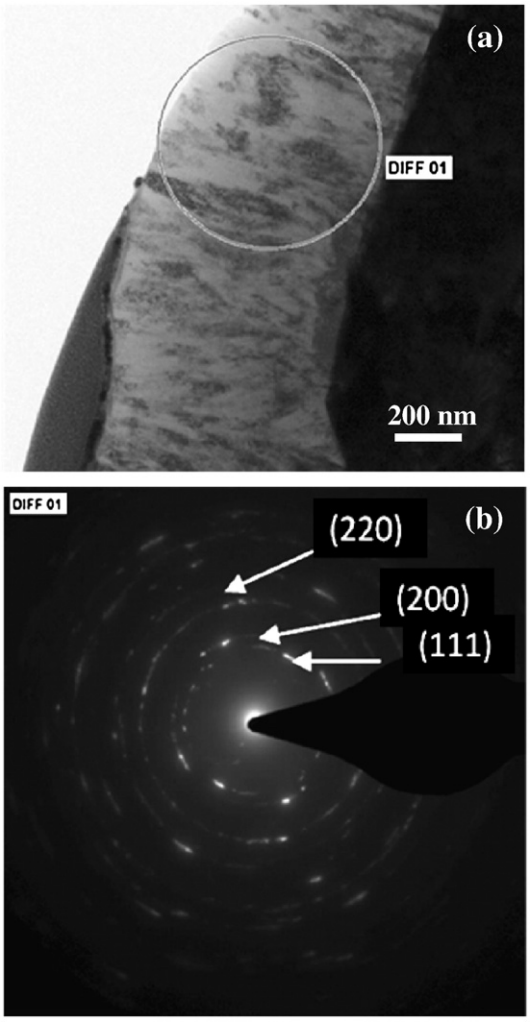

Fig. 3. (a) Bright field XTEM images from monolayer TiAlN coating (S1) and (b) the SAED pattern taken from the circle area in (a).

was consistent with the result reported by Vlasveld et al. [1]. The highest hardness value occurred at the Ti/Al concentration ratio = 50/50, which was consistent with the industrial application. Furthermore, the hardness of the Al-rich (S3) sample was the lowest one, which is in good aggrement with previous studies [5,14]. The multilayer films (S4–S6) consisting of alternative nanolayers with different concentrations exhibit an obvious difference in nanoindentation hardness. The conditions of S6 and S7 possess higher hardness in comparison with other conditions with similar performance to the monolayers (S2 and S3). Accordingly, subsequent study is focused on the conditions S6 and S7.

Fig. 2 shows the performance of BGA cutter with and without a coating film (S6). It is evident from Fig. 2 that such a coating film is good for the cutter to keep the accuracy of the slot width within 0.05 mm and is able to prolong the life of the tools before they were broken.

Fig. 3(a) presents a bright-field image of an XTEM specimen taken from a monolayer TiAlN coating (S1). It shows that its microstructure is similar to that of typical TiN coatings deposited by FCAIP with about 50-nm columnar structure containing diffused boundaries. Likewise, Fig. 3(b) shows the SAED pattern taken from the middle of the film indicated by the circle. The 111, 200 and 220 Bragg reflections were identified and were found consistent with the fcc-TiAlN phase (NaCl-B1 structure). XTEM specimen of the multilayer films (S6) is shown in Fig. 4(a), where the microstructure is different from that of S1 film. It consists of two clear interleaving nanolayers. The thickness is about

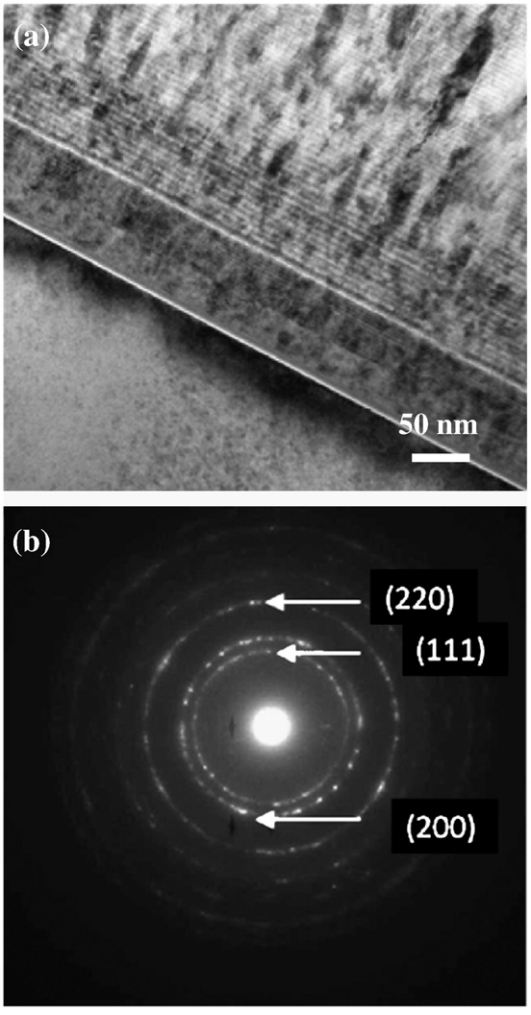

Fig. 4. (a) Bright field XTEM images from multi-nanolayer TiAlN coatings (S6) and (b) the corresponding SAED pattern of (a).

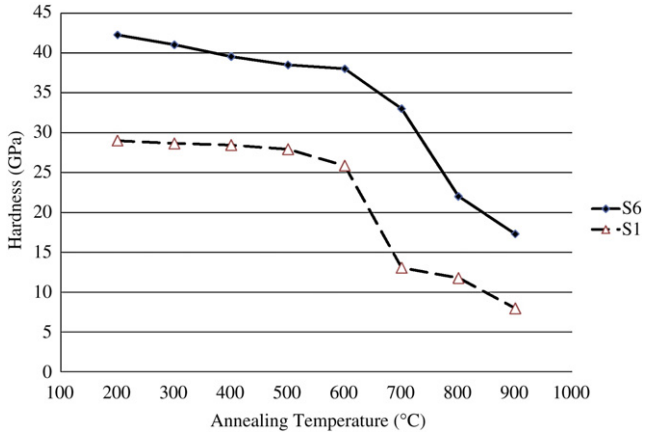

Fig. 5. Effect of annealing temperature on the nanoindentation hardness of multi-nanolayer TiAlN (S6) and monolayer TiAlN (S1) coatings.

5 nm (modulation wavelength is about 10 nm) and the columnar grain width is about 15 nm which is obviously smaller than the size of columnar grains in monolayer (S1). The different concentrations of TiAlN interface do not interrupt the grain growth, while the columnar grains were found to grow continuously through the interface. Since there are 111, 200 and 220 Bragg reflections found in the SAED pattern as shown in Fig. 4, the coexistence of two structures, fcc-TiAlN and HCP-AlN, as reported by Santana et al. [14] hence was not observed in the present study.

The above TEM analysis clearly reveals the difference between the monolayer film (S1) and the multilayer film (S6) in their grain size and shape. The columnar grain of S1 exhibits the grain width of about 50 nm and the length is almost the same as the thickness. In contrast, the columnar grain found in S6 has the columnar grain width of about 15 nm and the length of about 5 nm. According to previous study on nanostructured and nanocomposite strengthened materials [16]; the strengthening mechanism resulted from the difference in lattice structure or grain orientation. In the present study, the strengthening mechanism is ascribed to the decrease of the grain size and the densification of grain boundaries which, in turn, suppress the migration of dislocations. It is the same mechanism used in energetic ion bombardment. While there was no bias increase, it still had the same effect. The annealing treatments up to 900 °C in air were carried out to evaluate the sustenance of strength mechanism in multilayer film (S6) and monolayer film (S1). Fig. 5 shows that the multilayer film (S6) has higher hardness and declines abruptly at a temperature of 700 °C. The trend of the hardness change on the monolayer film (S1) is similar but with a lower level of hardness. The hardness decline may be caused by the grain growth and the decrease of grain boundary density, which end up with the loss of the hindrance of dislocation migration.

4. Conclusions

In the present study, monolayer and multilayer coatings were deposited by using Ti/Al targets with various concentration ratios *via* FCAIP process and their properties, performance and microstructures were investigated by nanoindentation hardness measurement, BGA cutter life test, TEM and annealing treatment up to 900 °C in air.

The multilayer TiAlN coatings (S6 and S7) consisting of the interleaving $Ti_{0.5}Al_{0.5}N$ and $Ti_{0.33}Al_{0.66}N$ nanolayers exhibit higher nanoindentation hardness in comparison with other samples prepared in this study. Further, during the machining of the BGA cutter coated with the multilayer TiAlN (S6), an effective extension of the life of accuracy by twice more than the one without the coating was observed. TEM analysis revealed that the multilayer TiAlN coatings possess smaller grains about 5 nm × 15 nm in size, which provide the

films with the similar strength mechanism as in nanocomposite films. The decrease in grain size and the densification of grain boundaries suppress the dislocation migration and thus enhance the mechanical properties of multilayer TiAlN coatings.

Acknowledgments

The authors gratefully acknowledge Prof. Jyh-Wei Lee of Tungnan University, Taiwan, R.O.C., for nanoindentation hardness measurement and Materials Analysis Technology Inc. at Chupei, Taiwan, R.O.C., for TEM specimen preparation and characterizations.

References

[1] A.C. Vlasveld, S.G. Harris, E.D. Doyle, D.B. Lewis, W.D. Munz, Surf. Coat. Technol. 149 (2–3) (2002) 217.
[2] H. Ohnuma, N. Nihira, A. Mitsuo, K. Toyoda, K. Kubota, T. Aizawa, Surf. Coat. Technol. 177–178 (2004) 623.
[3] H. Takaoka, E. Nakamura, T. Oshika, A. Nishiyama, Surf. Coat. Technol. 177–178 (2004) 306.
[4] J. Musil, S. Kadlec, J. Vyskocil, V. Valvoda, Thin Solid Films 167 (1988) 109.
[5] J. Musil, H. Hruby, Thin Solid Films 365 (1–3) (2000) 104.
[6] S. Veprek, M. Veprak-Heijman, P. Karvankova, J. Prochazka, Thin Solid Films 476 (1) (2005) 1.
[7] P.J. Martin, A. Bendavid, J.M. Cairney, M. Hoffman, Surf. Coat. Technol. 200 (7) (2005) 2229.
[8] A. Winkelmann, J.M. Cairney, M.J. Hoffman, P.J. Martin, A. Bendavid, Surf. Coat. Technol. 200 (14–15) (2006) 4213.
[9] H.C. Barshilia, K.S. Rajam, A. Jain, K. Gopinadhan, S. Chaudhary, Thin Solid Films 503 (1–2) (2006) 158.
[10] Y.Y. Chang, D.Y. Wang, C.Y. Hung, Surf. Coat. Technol. 200 (5–6) (2005) 1702.
[11] C.L. Chang, J.Y. Jao, W.Y. Ho, D.Y. Wang, Vacuum 81 (2007) 604.
[12] S.G. Harris, E.D. Doyle, A.C. Vlasveld, J. Audy, J.M. Long, D. Quick, Wear 254 (2003) 185.
[13] P.B. Mirkarimi, L. Hulman, S.A. Barnett, Appl. Phys. Lett. 57 (1990) 2654.
[14] A.E. Santana, A. Karimi, V.H. Derflinger, A. Schutz, Tribol. Lett. 17 (4) (2004) 689.
[15] G.M. Pharr, W.C. Oliver, MRS Bulletin 17 (7) (1992) 28.
[16] A.A. Voevodin, D.V. Shtansky, E.A. Levashov, J.J. Moore, Nanostructured Thin Films and Nanodispersion Strengthened Coatings, Kluwer Academic Publishers, Netherlands, 2004, p. 53.